# Path Integrals on the Lattice and Topological Actions

*DESY Summer Student Project, 2011*

Stephanie Hyland
*Trinity College Dublin, Ireland*

Marcus Sperling
*Technische Universität Dresden, Germany*

Supervisor
Karl Jansen


5th of September 2011

**Abstract**

We use methods of lattice field theories to investigate a simple 1-dimensional spin system with topological properties. We begin with an introduction to the theoretical foundations, including the Feynman path integral, Monte Carlo methods and in particular the Metropolis algorithm. The basic task of computing the value of $\langle x^2 \rangle$ in a Gaussian probability distribution is undertaken to introduce the methods, and to explain the problem of autocorrelation times. Motivation is then provided for our topological studies with a brief explanation of the role of $\chi_t$, the topological susceptibility, in explaining the anomalous mass of the $\eta'$ meson. We calculate $\chi_t$ for our system and compare it to analytical results in the continuum limit. Autocorrelation effects are found to be significant and freezing of the topological charge is observed. Open boundary conditions are introduced to ameliorate this problem. The energy gap $\Delta E = E_1 - E_0$ is obtained and also examined in the continuum limit. Finally, we suggest the cluster algorithm to reduce autocorrelation effects and briefly describe an alternative discretisation method to reduce non-zero lattice spacing issues.


# Contents

**1 Introduction and Theory** **1**
1.1 The Feynman Path Integral . . . 1
1.2 Relationship with Statistical Mechanics . . . 3
1.3 Monte-Carlo Methods . . . 4
1.4 Metropolis Algorithm . . . 5
1.5 Correlation . . . 6
1.6 General Remarks . . . 7

**2 An introductory example...** **7**
2.1 Analytical Solution . . . 7
2.2 Simulation Results . . . 8

**3 Topological Actions** **10**
3.1 Motivation . . . 10
3.2 The 1-d $O(2)$ model . . . 11
3.3 Computational Tasks . . . 11
3.4 Remarks: Statistics, Skipping and Boundary Conditions . . . 13
3.5 Topological Susceptibility . . . 14
3.6 Energy Gap . . . 18
3.6.1 Derivation . . . 18
3.6.2 Results . . . 19

**4 Improvements** **21**
4.1 Reducing the autocorrelation time - the cluster algorithm . . . 21
4.2 Reducing lattice artifacts - different discretisation . . . 22

**5 Conclusions** **23**

# 1 Introduction and Theory

Using theories on a lattice - that is, formulating these theories on a (Euclidean) space-time grid - has been established as a most valuable tool in quantum field theory and statistical mechanics to analyse and understand physical systems.

In particular, lattice methods have led to great success in the non-perturbative sector of quantum chromodynamics, where exact solutions are not possible. Using massively parallel supercomputers, observables for complex quark-gluon systems may be accurately determined and compared with experimental findings.

Motivated by these applications, we introduce the theoretical foundations of the lattice-based approach and apply it firstly to a simple example, and then to a system with topological properties. During our studies we also investigated the quantum harmonic oscillator, but the results are not included in this report. We refer the interested reader to the educational paper by Creutz and Freedman[1] for further discussion of this system.

## 1.1 The Feynman Path Integral

We begin with a key theoretical component - the path integral. This quantum mechanical formalism uses the concept of a 'sum over histories' to capture the dynamical properties of the system. In contrast to the canonical formalism, it does not require the use of operators on the Hilbert space. As we shall see, it has a natural relationship to discretised space-time, so one should not be surprised to see its extensive use in lattice-based theories.

Before deriving the path integral, we first consider the idea of the 'sum over histories' to gain some sense of the motivation for the approach. We begin with the classical concept of a single trajectory between endpoints and extend it (in the quantum fashion), to include all possible paths. This is simply the case for quantum mechanical processes, where the amplitude is given by a sum over alternative histories. The key point is that while each path contributes to the total amplitude, it contributes at a *different phase*. We see this in Feynman's original version of the 'integral',

$$K(b,a) = \sum_{\text{paths}} \text{const}\; e^{\frac{i}{\hbar}S[q(t)]} \tag{1}$$

where $K(b,a)$[1] is the quantum mechanical amplitude to reach a state $(b)$ from a state $(a)$.

If we accept this expression, and see that the phase is given by $i/\hbar S[q(t)]$, the classical limit is retrieved as $S \gg \hbar$. To see this more clearly, we note that small variations around a path giving an extremum in the action (ie, a classical path) will produce little change in the action, and thus the phase will be approximately constant. For 'quantum paths', these small variations produce huge fluctuations in phase, causing rapid oscillations between -1 and 1 which tend to cancel out the non-classical paths.

[1] This quantity is also called the 'propagator', as we shall see.

We are interested in the *propagator* between two points, $(t_i, q_i)$ and $(t_f, q_f)$ - the probability amplitude for the system being in state $(t_f, q_f)$ having been in state $(t_i, q_i)$. This is denoted by $\langle t_f q_f | t_i q_i \rangle$, and is equivalent to $K(t_f, q_f; t_i, q_i)$ in equation 1.

To calculate this quantity we split the time interval into $N$ discrete sub-intervals, each of width $\epsilon$. We then have

$$t_i = t_0, \qquad t_N = t_f, \qquad \epsilon N = t_f - t_i \tag{2}$$

Thus the connection with lattice calculations is apparent. This formalism suits our methods very well. We consider that the system has to pass through each time-point in the interval, such that the propagator becomes a product of incremental propagators, where the space-coordinates in each step are variable.

To encorporate all paths in our consideration, we integrate space at each time point between $-\infty$ and $\infty$, while fixing the endpoints at $q_i$ and $q_f$ (see figure 1.1). Mathematically, this looks like

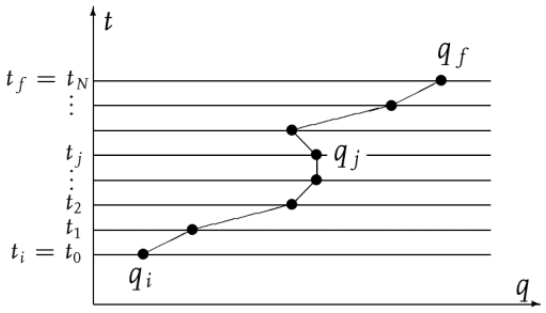


Figure 1: The time axis is divided into discrete intervals, and the $q_j$ values, corresponding to $q(t_j)$, take values between $-\infty$ and $\infty$. Image from [2].

$$\langle t_f q_f | t_i q_i \rangle = \int \dots \int \mathrm{d}q_1 \mathrm{d}q_2 \dots \mathrm{d}q_{N-1} \langle t_f q_f | t_{N-1} q_{N-1} \rangle \dots \langle t_j q_j | t_{j-1} q_{j-1} \rangle \dots \langle t_1 q_1 | t_i q_i \rangle \tag{3}$$

We can write the element $\langle t_j q_j | t_{j-1} q_{j-1} \rangle$ using the time evolution operator,

$$|t_j q_j\rangle = e^{\frac{i}{\hbar}\hat{H} t_j} |q\rangle$$

such that

$$\langle t_j q_j | t_{j-1} q_{j-1} \rangle = \langle q_j | e^{-\frac{i}{\hbar}\hat{H}(t_j - t_{j-1})} | q_{j-1} \rangle = \langle q_j | e^{-\frac{i}{\hbar}\epsilon \hat{H}} | q_{j-1} \rangle \tag{4}$$

For a typical Hamiltonian, after inserting a complete set of momentum states, we obtain

$$\langle q_j | e^{-\frac{i}{\hbar}\hat{H}(\hat{p},\hat{q})} | q_{j-1} \rangle \simeq \int \frac{\mathrm{d}p}{2\pi\hbar} \langle q_j | p \rangle \langle p | q_{j-1} \rangle e^{-\frac{i}{\hbar}H(p,q_k)} \tag{5}$$

We may use the fact that $\langle q_j | p \rangle = e^{ipq_j}$ to further simplify this expression. The Hamiltonian function $H(p, q_j)$[2] appears due to a choice in where to insert the momentum basis states. We could equally have made a different choice and obtained $H(p, q_{j-1})$. Since these choices are in our case arbitrary, a 'middle ground' is chosen for the resulting expression. Ultimately in the continuum limit, these considerations are unimportant. Combining all

[2]Note that the Hamiltonian is no longer an operator, but instead at this point a function of $(p, q_j)$, yielding a number.

of our bracket terms and collecting exponents in equation 5, we obtain that $\langle t_f q_f | t_i q_i \rangle$ is equal to

$$\lim_{\substack{\epsilon\to 0\\ N\to\infty}} \int \dots \int \mathrm{d}q_1 \dots \mathrm{d}q_{N-1} \frac{\mathrm{d}p_1}{2\pi\hbar} \dots \frac{\mathrm{d}p_N}{2\pi\hbar} \exp\left(\frac{i}{\hbar}\sum_{j=1}^{N}\left[p_j(q_j - q_{j-1}) - \epsilon H\left(pj, \frac{q_j + q_{j-1}}{2}\right)\right]\right) \tag{6}$$

Examining the expression in the exponential, we note that by extracting a factor of $\epsilon$, and taking the limit, we get

$$\begin{aligned}\lim_{\substack{\epsilon\to 0\\ N\to\infty}} \frac{i}{\hbar}\epsilon\sum_{j=1}^{N}\left[p_j\left(\frac{q_j - q_{j-1}}{\epsilon}\right) - H\left(p_j, \frac{q_j + q_{j-1}}{2}\right)\right] &= \frac{i}{\hbar}\int_{t_i}^{t_f} \mathrm{d}t\,(p\dot{q} - H(p,q)) \\ &= \frac{i}{\hbar}\int_{t_i}^{t_f} \mathrm{d}t L = \frac{i}{\hbar}S[q] \end{aligned} \tag{7}$$

For Hamiltonians quadratic in the momentum, the integration over momenta is simple, and we arrive finally at

$$\langle t_f q_f | t_i q_i \rangle \propto \int \mathcal{D}q e^{\frac{i}{\hbar}S[q]} \tag{8}$$

where

$$\int \mathcal{D}q = \lim_{\substack{\epsilon\to 0\\ N\to\infty}} \int \mathrm{d}q_1 \dots \mathrm{d}q_{N-1}$$

## 1.2 Relationship with Statistical Mechanics

The result we have obtained for the path integral is valid for Minkowski space. While we know that rapidly changing phase factors will tend to cancel out physically improbable paths, this effect is only apparent after performing the calculation. Using a technique called a 'Wick rotation' we may immediately distinguish those paths which do not contribute greatly to the propagator, while establishing an important relationship to statistical mechanics.

A Wick rotation transforms a problem in Minkowski space to one in Euclidean space by moving to imaginary time via the substitution $\tau = it$. After such a transformation, our path integral becomes

$$I = \int \mathcal{D}q e^{-\frac{1}{\hbar}S_E} \tag{9}$$

Clearly, unimportant paths are now exponentially suppressed. More interestingly, we see the formal similarity with a Boltzmann factor where $\hbar$ acts as a temperature. The $\hbar \to 0$ (classical) case, where quantum fluctuations are insignificant, is analogous to a $T \to 0$ case where statistical fluctuations in a physical system are 'frozen out'. Thus, quantum mechanics in imaginary time becomes statistical physics in real time. This is the power of the Wick rotation.

The connection established here motivates the use of the action for generating states with an appropriate distribution - this is the idea of 'importance sampling', which we use to perform Monte Carlo integrations.

## 1.3 Monte-Carlo Methods

The main problem in using the path integral formulation is that we have to evaluate the integral over the phase space $\mathcal{PS}$. However, these integrals might not be analytically solvable and therefore it is necessary to obtain numerical approximations. One suitable technique is called the *Monte-Carlo Method* or *Monte-Carlo Integration*. The purpose of this method is to approximate a definite integral using a finite number of randomly sampled points. More specifically, one wishes to make the approximation

$$\int_{\mathcal{PS}} f(x)\mathcal{D}x \simeq \sum f(x_i) \cdot \Delta x_i \tag{10}$$

where $x_i \in \mathcal{PS}$. The question is now how to choose these points $x_i$? Two possible ways are the following:

- Random Sampling: means that we choose the points $x_i$ randomly according to a uniform distribution over the whole phase space. This is problematic if, for example $\mathcal{PS}$ is very large. In this case a large number of points is needed to the cover the whole space. If it happens that not all regions of $\mathcal{PS}$ contribute equally - for example, in the case of a highly peaked probability distribution - then a lot of integration points will be wasted on unimportant areas.

- Importance Sampling: is designed to overcome this disadavntage. The idea is to generate phase space points $x_i$ which are not totally random, but instead more densely distributed in dominant regions of the phase space.

Let us now study the realisation of importance sampling in the content of path integrals. As seen previously in the connection to statistical physics, the action $S$ can be regarded, like a Boltzmann factor, as the generator of a probability distribution $P(x) \sim e^{-S}$. Therefore, the expectation value of some observable $A$ is, within the notation of statistical physics,

$$\langle A \rangle = \frac{\int A(x) e^{-S(x)} \mathcal{D}x}{\int e^{-S(x)} \mathcal{D}x} \tag{11}$$

In this case, the normalised probability distribution[3] is $P(x) = \frac{e^{-S(x)}}{\int e^{-S(x)} \mathcal{D}x}$, with $\int P(x)\mathcal{D}x = 1$. The idea is now to somehow generate points $x_j \in \mathcal{PS}$ according to this distribution $P(x)$, i.e.:

$$P(x_j)\mathcal{D}x = \frac{e^{-S(x_j)}\mathcal{D}x}{\int e^{-S(x)}\mathcal{D}x} \tag{12}$$

Hence, the Monte Carlo estimate $\bar{A}$, with points distributed in the above manner, of the expectation value $\langle A \rangle$ is given by:

$$\bar{A} = \frac{1}{N} \sum_{i=1}^{N} A(x_i) \qquad \{x_i \in \mathcal{PS} : i \in \{1, 2, ..., N\}\} \tag{13}$$

where $N$ is the total number of points generated according to the distribution above.

[3] Recalling that $S(x)$ is the action of our system, we see that this distribution will tend to select more points which minimise the action - a physically desirable result.

## 1.4 Metropolis Algorithm

We have seen that importance sampling is the desired method to choose points with an appropriate distribution for approximating physical quantities. However, the specific implementation has to be discussed in further detail. We need to know how to generate these points. One realisation is the so-called *Metropolis Algorithm* which will be the subject of this section and is also the basis for all subsequent programming steps.
The best way to explain the algorithm is pseudo code:

1. Let $S(x)$ denote the action of the system under consideration, $d$ a variable simulation parameter, and $x_i$ old point or starting point.

2. Choose randomly (with uniform probability) the new point (proposal) $x_i'$ such that $x_i' \in [x_i - d, x_i + d]$.

3. Compute the difference in action between the new and old 'configuration'[4],

$$\Delta S(x_i', x_i) := S(x_i') - S(x_i)$$

4. The decision step is realised by the following:

<table>
<tr><td rowspan="2">IF $\Delta S(x_i', x_i) < 0$<br>THEN accept $x_i'$</td><td colspan="2">IF $\Delta S(x_i', x_i) \geq 0$<br>THEN randomly $r \in [0, 1]$</td></tr>
<tr><td>IF $\Delta S(x_i', x_i) > r$<br>THEN accept $x_i'$</td><td>IF $\Delta S(x_i', x_i) \leq r$<br>THEN reject $x_i'$</td></tr>
</table>

   The term 'accepted' means that the proposal will be the starting point for the next iteration step: $x_{i+1} = x_i'$. 'Rejected' means that in the next step we still have the same old point, i.e. $x_{i+1} = x_i$.

An important point to realise is that we have to use the Metropolis algorithm several times to find the appropriate sample of points $\{x_j\}$. Another way of describing this is to say that each time we apply the Metropolis algorithm to an old 'configuration' $x_j$ we get an proposal $x'_j$. This point is eventually accepted (if it leads to a decrease in action or with a certain probability if $\Delta S(x'_j, x_j) \geq 0$)[5].

After repeating this step several times we get a configuration $\{x_{eq}\}$ which is closer to the desired equilibrium distribution $P(x)$ in the sense that the distribution of the points $\{x_{eq}\}$ resembles $P(x)$ . This sample $\{x_{eq}\}$ can then be used to compute the Monte Carlo estimate for the expectation value.

This can also be understood in physical terms. The relaxation of the configurations into equilibrium corresponds to *thermalisation*, because the system starts at some chosen starting configuration and evolves over (iteration-) time into the equilibrium configuration. This is analogous to the situation described above.

[4] Here our configuration consists of a single point. Later, we consider the complete path of a particle with specified boundary conditions as a single configuration.

[5] This condition enables the system to escape from local minima in the action. In statistical mechanics, it can be thought of as resulting from the finite temperature of the system.

## 1.5 Correlation

For the later applications, mostly in analysing and evaluating the reliability of our simulation data, we need to consider some systematic effects due to the nature of the Metropolis Algorithm. We speak of the *correlation* (more specifically autocorrelation) between different configurations. We can think of this as giving some measure of how related the different configurations are to each other.

We are aiming for a sample of configurations of the system such that these configurations are distributed according to the desired probability distribution and also are independent of each other. This independence condition is important and necessary to obtain good statistical results and to lose independence of the initial conditions.

The design of the above algorithm suggests that we are dealing with an ideal *Markov process*. Markov processes (or chains) are often used to model the configurations of a system within the assumption of limited dependence. This means that successive configurations can only depend on a finite number of previous steps - ideally only the previous one.

However, in the case of the Metropolis algorithm, we find that the configurations always have some residual dependence on previous states. A factor in this is the chosen parameter $d$, which determines how quickly we can obtain an entirely new configuration. As we shall see, the choice of $d$ is not a trivial matter.

Thus, we need to investigate the 'autocorrelation' of our configurations $\{x\}_j$ to have an idea of the extent of these residual effects, and to take them into account while performing error analysis.

In general, the correlation between two continuous functions $g, h : \mathbb{R} \to \mathbb{R}$ is given by the integral[3]

$$\mathrm{Corr}(g,h)(\tau) := \int_{-\infty}^{\infty} g(t+\tau) \cdot h(t) \mathrm{d}t$$

Which resembles the definition of the convolution of $g$ and $h$. Nevertheless, for discrete sequences $g_k$ and $h_k$ (which have to be periodic in $N$), the correlation is given as:

$$\mathrm{Corr}(g,h)(j) := \sum_{k=0}^{N-1} g_{k+j} \cdot h_k$$

However, the correlation describes how similar those two functions or sequences are. Which means that the correlator is ideally zero if there is no connection between the data. On the contrary, we need to investigate the dependence of the data of itself. Therefore, we compute the correlation of the finite sequence $\{x_j\}$ with itself. Let us consider for simplicity a 1-dim. configuration $x$ with a given number of iterations $N$, i.e. $j \in \{1, 2, ..., N\}$. Since we do not have periodicity, we normalise the correlation:

$$C(j) := \frac{1}{N_j^*} \cdot \sum_{k=1}^{k+j \leq N} x_{k+j} \cdot x_k$$

where $N_j^*$ is the number of summations obeying $k + j \leq N$ for a given $j \in \mathbb{N}$.
As shown by Buendía[4][6], we expect the autocorrelation function for the Metropolis algo-

[6]While this paper discusses the autocorreation function for the Langevin algorithm, the principle is the same for the Metropolis algorithm.

rithm to have an exponential decay of the form

$$C(t) \sim e^{-\frac{t}{\tau_{ac}}} \tag{14}$$

Where $\tau_{ac}$ is the so-called autocorrelation time.

### 1.6 General Remarks

For the implementation of the algorithm and all of the following systems we wrote two independent programs using either *C* or *FORTRAN* as the programming language. The advantage of this strategy is that it is possible to cross-check results, avoid bugs and improve the code.

## 2 An introductory example...

In order to get acquainted with Monte Carlo methods, Metropolis Algorithm and Importance Sampling, we consider the following task:

Compute the expectation value of $x^2$ within the normalised probability distribution:

$$P(x) = \frac{e^{-x^2}}{\int_{-\infty}^{\infty} e^{-x^2}\mathrm{d}x} \tag{15}$$

and compare the results with the analytical solution.

### 2.1 Analytical Solution

The expectation value of $x^2$ is given as:

$$\langle x^2 \rangle := \int_{-\infty}^{\infty} x^2 \cdot P(x)\mathrm{d}x$$

Looking at the first part of the integral, and splitting the limits, we get

$$\begin{aligned} I &= \int_{-\infty}^{\infty} x^2 e^{-x^2}\mathrm{d}x = \underbrace{\int_0^{\infty} x^2 e^{-x^2}\mathrm{d}x}_{t:=x^2, x\geq 0} + \underbrace{\int_{-\infty}^{0} x^2 e^{-x^2}\mathrm{d}x}_{s:=x^2, x<0} \\ &= \frac{1}{2}\int_0^{\infty} \sqrt{t} e^{-t}\mathrm{d}t - \frac{1}{2}\int_{\infty}^{o} \sqrt{s} e^{-s}\mathrm{d}s = \int_0^{\infty} t^{\frac{3}{2}-1} e^{-t}\mathrm{d}t = \Gamma\left(\frac{3}{2}\right) \end{aligned}$$

We now prove the following property of Gamma function $\Gamma(z+1) = z \cdot \Gamma(z)$:

$$\begin{aligned} \Gamma(z+1) = \int_0^{\infty} t^{z+1-1} e^{-t}\mathrm{d}t &= -t^z e^{-t}|_{t=0}^{t=\infty} + z\int_0^{\infty} t^{z-1} e^{-t}\mathrm{d}t \\ \text{where} \quad \lim_{t\to 0} -t^z e^{-t} &= 0 \quad \text{and} \quad \lim_{t\to\infty} -t^z e^{-t} = 0 \\ \text{as} \quad t^z e^{-t} &= e^{z\ln t - t} \to 0 \quad \text{as} \quad t \to \infty \end{aligned}$$

Hence we get $I = \Gamma\left(\frac{3}{2}\right) = \frac{1}{2}\Gamma\left(\frac{1}{2}\right)$. Furthermore, we know the value of the Gaussian integral and can apply the same steps as above to obtain:

$$\int_{-\infty}^{\infty} e^{-x^2}\mathrm{d}x = \Gamma\left(\frac{1}{2}\right) = \frac{\sqrt{\pi}}{2}$$

Thus, the analytical solution is: $\langle x^2 \rangle = \frac{1}{2}$.

## 2.2 Simulation Results

The simulation of this system requires only three parameters:

- $d$, determining the range of the proposal
- $N_{iter}$, the number of iterations
- $x_0$, the starting point

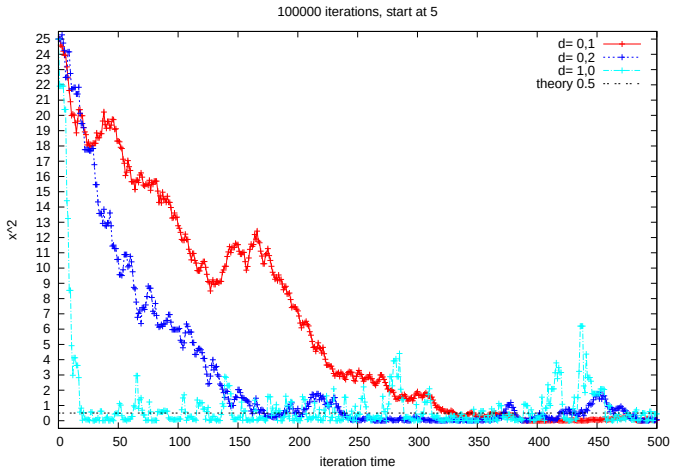


Figure 2: Value $x^2$ going into equilibrium for different values of the increment $d$.

First, we look at the behaviour of $x^2$ as function of the iteration time with respect to different values of the increment $d$ (see fig. 2). As we can see, the value of the parameter $d$ clearly influences how fast the system thermalises (settles into equilibrium) if we have a badly chosen starting point. This means that if we have no idea about the equilibrium configuration (e.g. no analytical solution) then we might want to take a large value of $d$ to reach equilibrium faster. On the other hand, if we look at the fluctuations around the analytical solution then we realise that overly large values of $d$ lead to averages with large errors.

Before the analysis of further results, it is necessary to define the acceptance rate $R$ of the Metropolis Algorithm by:

$$R := \frac{\text{number of accepted proposals}}{\text{total number of proposals}} \tag{16}$$

The choice of $d$ is crucial, as seen above. In order the determine the appropriate value it is necessary to look at the autocorrelation time $\tau_{ac}$ and the acceptance rate $R$ as functions of $d$ (see figure 3).

First, we focus on figure 3a where the autocorrelation function for different $d$ is shown. The most immediately apparent behaviour is the exponential decay, as predicted by equation 14. To obtain $\tau_{ac}$ from the simulation data we use the open source program **R** with library *hadron* and the *uwerr* function. Extracting the values of $\tau_{ac}$ from the autocorrelation functions, we can compare them and $R$ as functions of $d$ in one graph (see fig. 3b). We observe three different regions:

- $d \leq 1$: The acceptance rate rapidly approaches one, while the autocorrelation time strongly increases as $d \to 0$. This suggests that one should avoid this region for the following reason: due to the small range of proposals, the probability of randomly selecting a point which is accepted is high. In detail, the probability of choosing a

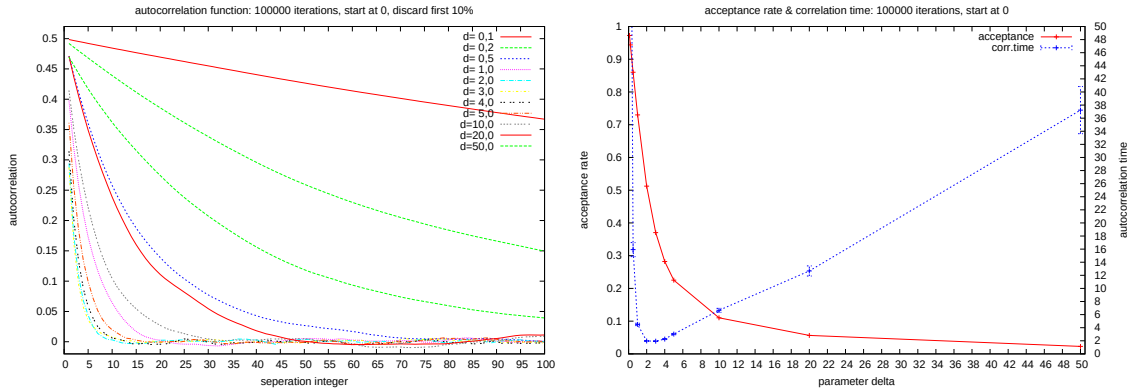


Figure 3: Left: correlation for different $d$ ; Right: acceptance rate and autocorrelation time for different $d$

point with decreasing action or similar action is high. Hence, if we have a slight increase in action: $\Delta S \ll 1 \Rightarrow e^{-\Delta S} \approx 1 - \Delta S$, which implies that the point is accepted for most of the random variables $r$ of the Metropolis Algorithm. However, since $d$ is so small, the configurations are highly correlated which leads to a large $\tau_{ac}$.

- $d \geq 5$: $R$ decreases and $\tau_{ac}$ increases as $d$ increases. This behaviour is due to the large range of new proposals. It follows that probability of choosing a point with increasing action is high. The consequence is the rejection of most of the proposals, and a low acceptance rate. Since a configuration is repeated when the proposal is rejected, this results in an increasing autocorrelation time, as subsequent configurations are identical.

- $1 < d < 5$: This region seems to be the appropriate range of $d$ values for our simulations, as the autocorrelation length is small (configurations become independent quickly) and the acceptance is between $20\% - 50\%$ (which ensures fast thermalisation).

Since we wish to choose $d$ such that

1. The acceptance rate $R$ is not too small and

2. The autocorrelation time $\tau_{ac}$ is as small as possible

we conclude from this analysis that $d \approx 2$ is appropriate, as $\tau_{ac} \approx 2$ and $R$ is still over 50%. We fix $d$ at 2 for all subsequent simulations.

For the computation of $\langle x^2 \rangle$ by equation 13, we average our function $f(x) = x^2$ over the points $x_i$ which are distributed according to the probability distribution 15. We know that the points $x_i$ have taken on this equilibrium distribution when the system is thermalised. Thus we must only start averaging after this point has been reached. Determination of this point is not exact, and is based on examining a graph such as figure 2. Having done so, we find our simulation to produce approximated values of $\langle x^2 \rangle$ which agree well with the analytical solution.

# 3 Topological Actions

## 3.1 Motivation

Before going into the details of the model we have considered, it is useful to spend some time on the motivation for topological theories.

Consider the following mesons $\eta$, $\eta'$ and $K$ and their quark content[7]:

| meson | composition | approx. mass |
|---|---|---|
| $K^0$ | $d\bar{s}$ , $s\bar{d}$ | 498MeV |
| $K^+$ | $u\bar{s}$ | 494MeV |
| $K^-$ | $s\bar{u}$ | 494MeV |
| $\eta$ | $u\bar{u}$ , $d\bar{d}$ , $s\bar{s}$ | 548MeV |
| $\eta'$ | $u\bar{u}$ , $d\bar{d}$ , $s\bar{s}$ | 958MeV |

The approximation of the mass of the $\eta$ and $\eta'$ by using the quark-content of the $K$'s and the mass of the $u$ quark ($m_u \approx 1.7 - 3.3\text{MeV}$) yields:

$$m_\eta \approx m_{\eta'} \approx \langle m_K \rangle + 2 \cdot m_u \leq 500\text{MeV} + 2 \cdot 3.3\text{MeV} < 510\text{MeV}$$

With this estimation it is already difficult to justify the $\eta$ mass, but by no means is it possible to explain the huge mass of $\eta'$. The quark model seemingly cannot explain this puzzle. However, there is an amazing mechanism arising from topological effects of gluon field configurations which is believed to provide the very large mass of the $\eta'$ meson. We may better understand the notion of topological effects by considering objects called *instantons*. Mathematically, these are classical solutions to Yang-Mills equations minimising the energy of the system with topologically nontrivial properties[5]. These properties are described by a quantity called the *topological charge*, a quantum number related to nontrivial homotopic properties of the system, which can intuitively be understood as a kind of 'winding number' for the solution.

The result is that it is possible to explain the anomalous mass of the $\eta'$ using these topological considerations[6].
In addition, there exists the remarkable *Witten-Veneziano formula*[8]

$$\frac{f_\pi^2}{2N_f}\left(m_\eta^2 + m_{\eta'}^2 - 2m_K^2\right) = \chi_{top}$$

which connects physical quantities (the masses of the mesons, $m_K$, $m_\eta$, $m_{\eta'}$) with a purely topological quantity, called the *topological susceptibility* $\chi_{top}$, which measures the fluctuation of the topological charge.

However, instead of looking at the very demanding model of QCD itself, this report will continue with a simpler, but illustrative model. We will find that problems encountered in much more sophisticated systems also appear in this one dimensional model. Therefore, the analysis of these phenomena will be the main part of this section.

[7] The mesons are actually a superposition of these quarks.
[8] Here $N_f$ is the number of quark flavours, and $f_\pi$ is a pion decay factor.

### 3.2 The 1-d $O(2)$ model

We start with an overview of the system in question. This is a 1-d $O(2)$ spin system, equivalent to the quantum mechanical rotor[7] and analytically solvable in the continuum (see [7],p.5). 1-d refers to the fact that the system is fixed in space and $O(2)$, the orthogonal group of $2 \times 2$ matrices, to its rotational freedom. The basic principle of the rotor is a particle with mass $M$ constrained to move on a circle with radius $R$, having a moment of inertia $I = MR^2$. The coordinate degree of freedom we consider is $\varphi$, the angle describing the postion of the particle on the circle (or equivalently, the orientation of the spin). We define $\beta = \frac{1}{T}$ (where $T$ is the 'temperature' of the system), which becomes the volume of our time-lattice in its discretised form.

The Euclidean continuum action is

$$S[\varphi] = \int_0^\beta \mathrm{d}t \frac{I}{2}\dot{\varphi}^2 \tag{17}$$

We introduce the topological charge for this system as:

$$Q[\varphi] = \frac{1}{2\pi}\int_0^\beta \mathrm{d}t\dot{\varphi} \in \mathbb{Z} \tag{18}$$

Using periodic boundary conditions, this charge is simply the number of complete revolutions the rotor/spin makes in the specified time period, with an associated direction.

In addition, we list some necessary relations and quantities without further justification[9]:

1. Define the topological susceptibility by $\chi_t := \frac{<Q^2>}{\beta}$
2. In the limit $\beta \to \infty$ we get the connection: $\chi_t = \frac{1}{4\pi^2 I}$
3. Define the correlation length[10] $\xi$ and obtain, again in the $\beta \to \infty$ limit, the energy gap between ground state and first excited state: $\xi = \frac{1}{E_1 - E_0} = 2I$ (see section 3.7.1 for derivation)

### 3.3 Computational Tasks

As already mentioned, the system under consideration can be equivalently regarded as a spin variable $\varphi \in (-\pi, \pi]$. We let the spin evolve in time (i.e. $\varphi = \varphi(t)$) and want to compute the action $S[\varphi]$ (see eqn. 17) between fixed time endpoints. A discrete time lattice with lattice spacing $a$ and number of timepoints $N_{path}$ is introduced[11], such that $\beta = a \cdot N_{path}$. Hence the continuous $\varphi(t)$ turns into a finite set of spin orientations $\{\varphi(a \cdot j) : j \in \{0, 1, ..., N_{path} - 1\}\}$. Furthermore, it is necessary to discretise the time derivative of $\varphi$. For simplicity, let $\varphi_j := \varphi(a \cdot j)$:

$$S[\varphi] = \int_0^\beta \mathrm{d}t \frac{I}{2}\dot{\varphi}^2 \to \frac{I}{2}\sum_{j=0}^{N_{path}-1} \dot{\varphi}_j^2 \cdot a$$

[9] We direct the interested reader to Bietenholz et al.[7], where this model is discussd in detail.

[10] Note: this is *not* related to the correlation functions over Monte Carlo iterations we discussed earlier. This arises from correlation functions over physical, and not Monte Carlo time, and has physical meaning for the system.

[11] We have already seen this procedure in section 1.1

where one can choose a simple way of discretising the derivative by:

$$\begin{aligned} \varphi(t+a) &= \varphi(a) + \dot{\varphi}(t) \cdot a + \frac{1}{2}\ddot{\varphi}(t) \cdot a^2 + O(a^3) \quad \text{by Taylor Theorem} \\ \Rightarrow \quad \dot{\varphi}_j &= \frac{\varphi_{j+1} - \varphi_j}{a} + O(a) \end{aligned} \tag{19}$$

Consequently, the discrete action has the following form:

$$S[\varphi] = \frac{I}{2a} \sum_{j=0}^{N_{path}-1} \left( (\varphi_{j+1} - \varphi_j) \mod 2\pi \right)^2 \tag{20}$$

In the same way one gets for the topological charge (see eqn. 18):

$$Q = \frac{1}{2\pi} \sum_{j=0}^{N_{path}-1} \left( (\varphi_{j+1} - \varphi_j) \mod 2\pi \right) \in \mathbb{Z} \tag{21}$$

Figure 4 provides examples demonstrating paths with different topological charges. A longer time path had to be taken to demostrate the $Q = 3$ case, as this charge is very unlikely for short paths.

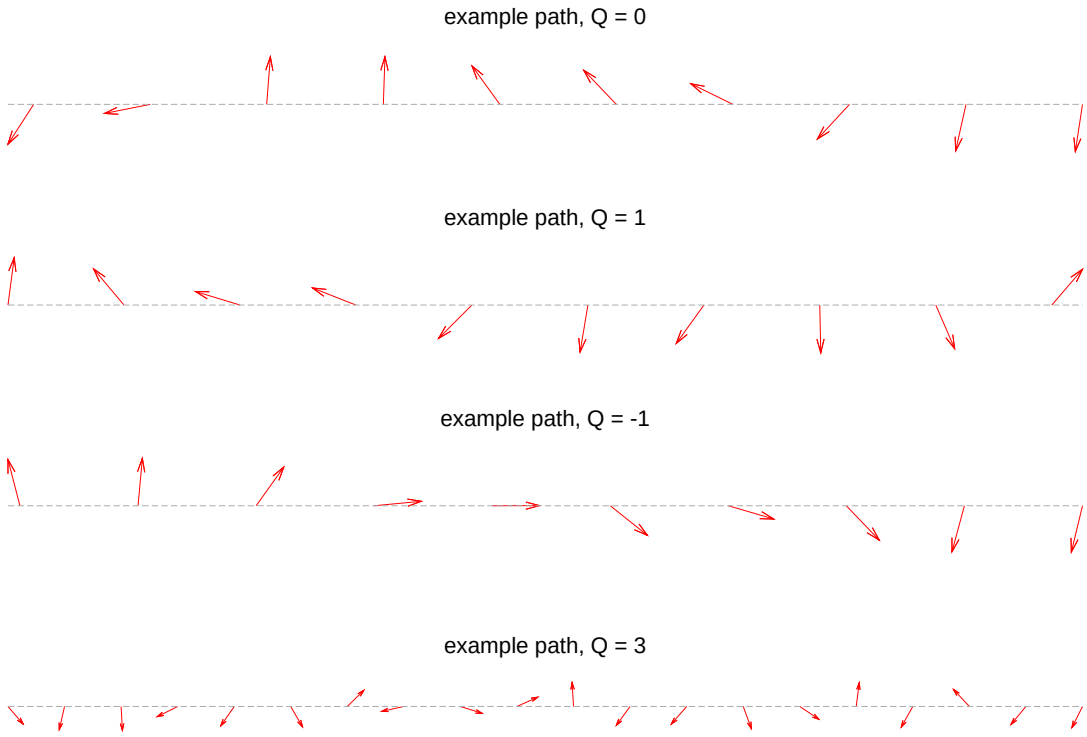


Figure 4: Examples of paths with various topological charges. Time goes from left to right, with periodic boundary conditions. These are purely illustrative examples, as paths used in simulations contain orders of magnitude more points.

Before continuing to the next section, some remarks about the implementation of the model are appropriate: The main difference compared to the simple first system is the

extension of the algorithm from a configuration consisting of a single point, to one given by a path of points separated on a time lattice. This is realised as seen in figure 5.[12]
The algorithm now goes as follows:

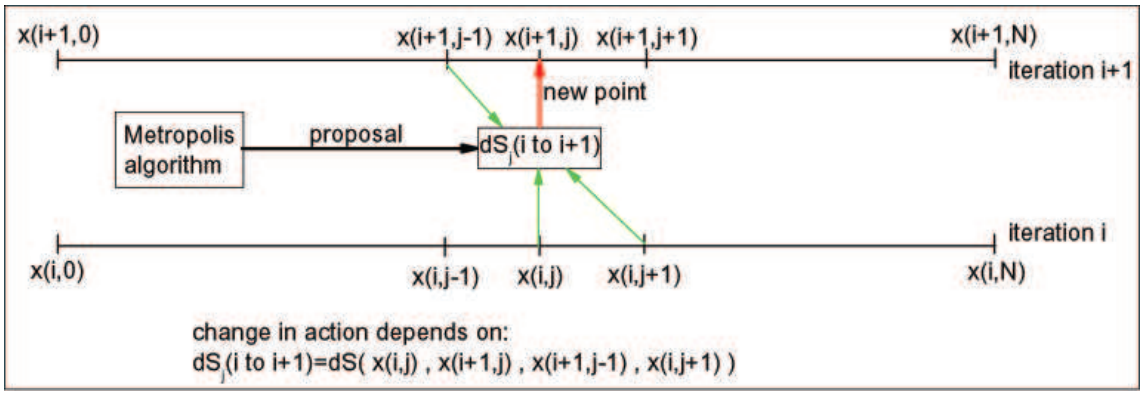


Figure 5: realisation of Metropolis Algorithm for a path

1. Create a starting configuration: i.e. $\{x(0,j) : j \in \{0,1,...,N\}\}$
2. At the updating step for $x(i,j)$ to $x(i+1,j)$[13], the following configurations are compared to each other:

$$\begin{aligned} \mathbf{x} &:= \{x(i,0), x(i,1), ..., x(i,j-1), x(i,j), x(i,j+1), ..., x(i,N)\} \\ \mathbf{x}' &:= \{x(i+1,0), x(i+1,1), ..., x(i+1,j-1), \tilde{x}, x(i,j+1), ..., x(i,N)\} \end{aligned}$$

   Where $\mathbf{x}$ corresponds to the old configuration and $\mathbf{x}'$ to the partially updated configuration with the new proposal $\tilde{x}$ for the point $x(i,j)$.

3. Perform the normal decision step $\Delta S(\mathbf{x}', \mathbf{x})$, like in the zero dimensional case.

It is important to realise that we need not compute the full action for the configuration at each step. Since the 'interaction' between neighbouring timepoints is of first order (that is, only nearest neighbours contribute) $\Delta S(\mathbf{x}', \mathbf{x})$ depends only on three points - $x(i,j), x(i,j+1), x(i+1,j-1)$ and the proposal. This local character in the action enables us to perform the Metropolis algorithm orders of magnitude faster than having to calculate the full action at each step.

### 3.4 Remarks: Statistics, Skipping and Boundary Conditions

As shown in previous sections, the autocorrelation time presents a problem for generating truly independent configurations and hence for averaged quantities. Since we can only consider independent configurations in our Monte Carlo averages, an autocorrelation time greater than one reduces our effective statistics. An idea to overcome this problem would be to increase the number of iterations $N_{iter}$ by the order of $\tau_{ac}$ to regain the desired number of independent measurements. We define a fixed number of measurements for good statistical

[12] The notation $x(i,j)$ refers to the spin variable $\varphi(t)$ at iteration step $i$, at time position $j$ on the lattice.
[13] At this point, all spins $x(i+1,k)$ for $k \in \{0, j-1\}$ have already been updated.

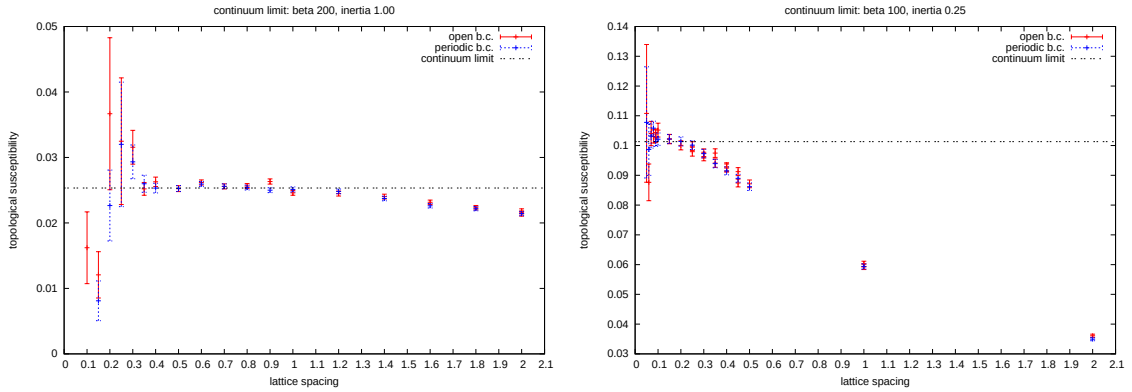


Figure 6: continuum limit: left graph: $\beta = 200$, $I = 1,00$ and $d = 2$; right graph: $\beta = 100$, $I = 0,25$ and $d = 2$

results, and vary the number of iterations depending on the autocorrelation length (we try to choose $l_{corr} \geq \tau_{ac}$),

$$N_{iter} = N_{measure} \cdot l_{corr}$$

In our simulation, we only take into account every $l_{corr}$th configuration for calculating the observables, thus ensuring independent measurements.

However, this presents immediate computational problems, greatly increasing the time it takes for simulations to run. For a simple system such as ours, this is not an unsurmountable problem, but for highly complex QCD calculations, this 'brute force' method is not a viable solution. We must find a better way to reduce the autcorrelation time. One method is with a special choice of boundary conditions, which we introduce now.

Formulae 20 and 21 indicate that it is necessary to deal with boundary conditions, since we have a finite system. The boundary conditions affect especially terms like $\varphi_{-1}$ and $\varphi_{N_{path}}$. A discussion of two different types of boundary conditions (b.c.'s) is appropriate:

- Periodic: the principle requirement is $\varphi_0 = \varphi_{N_{path}}$. This yields two statements:

$$\varphi_{-1} := \varphi_{N_{path}-1} \wedge \varphi_{N_{path}} := \varphi_0$$

- Open: According to Lüscher et al.[8], *open boundary conditions* may be used to reduce the problem of autocorrelation times. The idea is that $\varphi_0$ has no left neighbour, i.e. there are no terms like $(\varphi_0 - \varphi_{-1})$ and, similarly, $\varphi_{N_{path}-1}$ has no right neighbour.

## 3.5 Topological Susceptibility

As we have mentioned earlier, one interesting observable of the spin-system is the topological susceptibility. In particular, we want to consider the continuum limit, which means the following:

$$(a \to 0) \wedge (N_{path} \to +\infty) \quad \text{with the constraint:} \quad \beta = a \cdot N_{path} = const$$

We ran the simulation for two different set of parameters $((I = 1, \beta = 200), (I = 0.25, \beta =$

100)) as can be seen in figure 6. The left graph shows the results for open and periodic boundary conditions with a fixed number of measurements of $100,000$ and the right graph with $10,000$ measurements. Although both graphs in figure 6 seem to show different behaviour, it is possible to rescale the $a$-axis as follows: going back to equation 20 to pick up the coefficient of $\frac{I}{2a}$. For two sets of paramaters $(I_1, a_1)$ and $(I_2, a_2)$, it it possible to transform one into the other, in the sense that we can rescale one to have the same $a$ axis.

$$\frac{I_1}{a_1} = \frac{I_2}{a_2} \Rightarrow a_1 = \frac{I_1}{I_2} \cdot a_2$$

The combined plot can be seen in fig. 7. One observes a resemblance in the behaviour for

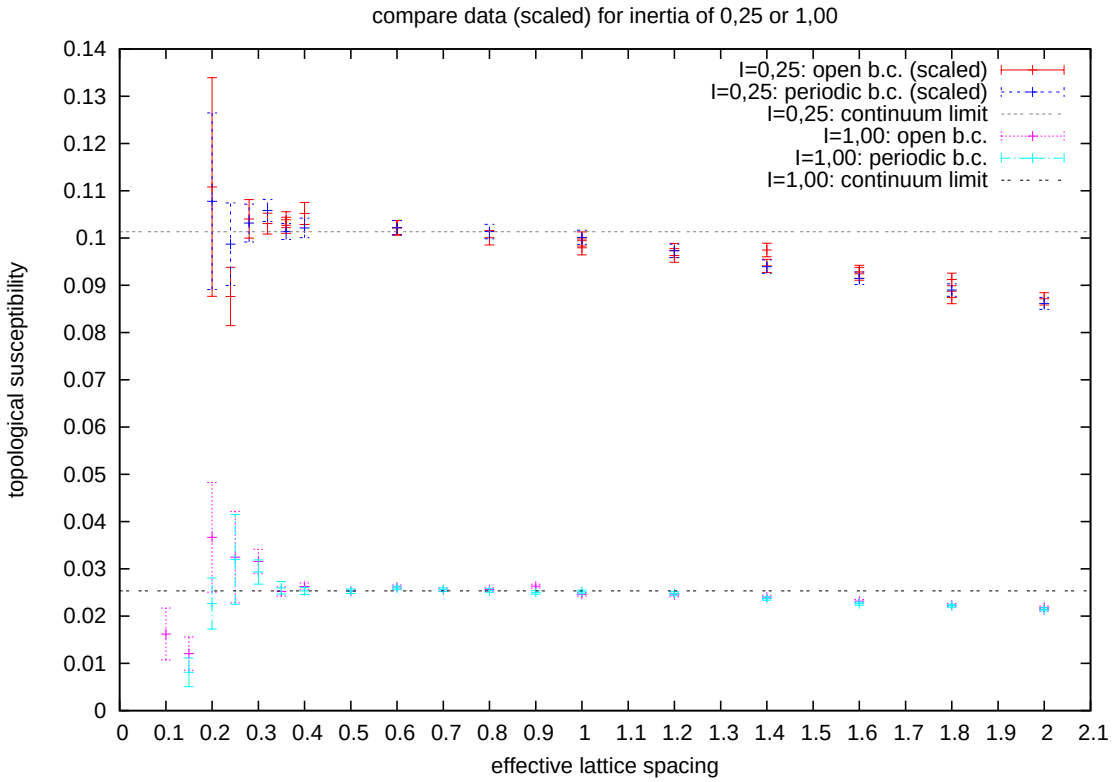


Figure 7: continuum limit for $(\beta = 100, I = 0,25)$ and $(\beta = 200, I = 1,00)$ with scaled $a$ axis for $I = 0,25$

both parameter sets and roughly three different regions may be determined:

1. $a \in (1, 2]$: the continuum limit is not reached within the errors
2. $a \in (0.35, 1]$: the data is in agreement with the continuum limit
3. $a \in (0, 0.35]$: the errors are increasing rapidly and no definite conclusion for the continuum limit can be reached.

The explanation for these behaviours is the following:

- The first region (1) is due to finite lattice spacing effects, that is, the manner in which the derivative $\dot{\varphi}$ has been discretised (see equation 19) produces lattice artifacts,

deviations of order $a$. This explains the observed deviations from the continuum value of $\chi_t$.

- In the second region (2) the data agrees well with the theoretical expectation.
- Last, we focus on the region for the smallest lattice spacings (3). To understand the behaviour there, it is necessary to look at the topological charge $Q$ as a function of iteration time at different lattice spacings (see figure 8).

Examining figure 8 yields the following analysis:

- For relatively large lattice spacings ($a \geq 0.5$) the topological charge oscillates around 0 over iteration time. This is because one may expect that the topological charge is Gaussian distributed. Indeed, this is reflected by the histogram in figure 8g.
- For smaller lattice spacings ($a \approx 0.05$) one recognises a change in the graph. It is no longer clearly distributed around zero. We begin to see the effects of autocorrelation as the topological susceptibility 'wanders' for hundreds of thousands of iterations in approximately the same direction.
- Finally, for very small spacings ($a \approx 0.01$) the topological charge is *frozen*. This means that it is constant over several $100,000$ or even $1,000,000$ iteration steps. This is seen most dramatically in figure 8e, where the topological charge is fixed at 3 for over 15 million iterations. The reason for this lies in the action (equation 20), where we observe a dependence of $\sim \frac{1}{a}$. The consequence is that the change in action becomes very large unless the change in the angle is very small. We then have that new points are simultaneously unlikely to be accepted (which increases the effective autocorrelation time as we have seen, thus effectively reducing our statistics), and those which are accepted cannot significantly alter the spin configuration. Since the $\langle Q^2 \rangle$ is a measure for the fluctuation of $Q$, and $Q$ is constant over millions of iterations, we cannot get a reliable value of $\chi_t$.

In addition, a more detailed discussion about open and periodic boundary conditions is appropriate. As seen in figure 8, the freezing of the topological charge at small lattice spacings is a serious problem for periodic b.c's which is difficult to overcome. One idea suggested by Lüscher et al.[8], is to use the open boundary conditions we introduced above. In the case of periodic boundary conditions one requires $x_0 = x_{N_{path}}$. This makes it difficult to change to a configuration with a different $Q$ and leads to the freezing of the topological charge. An intuitive explanation for this is to imagine trying to remove the twist in a closed belt - impossible without first separating the ends. As Lüscher et al. describe it, open bounary conditions enable the topological charge to smoothly 'flow' in and out of the system. The expectation for open b.c.'s is to obtain better results for smaller lattice spacings and to extend the limit until which we can compute reliable values.

Indeed, if we compare the results for $a = 0.01$ between open and periodic boundary conditions, the difference is remarkable. While the open b.c.'s display significant autocorrelation effects, the topological susceptibility is not entirely frozen, as in the case for periodic boundary conditions. We see the problem is, if not solved (we find open b.c.'s to break down eventually in the continuum limit), then ameliorated by the choice of boundary conditions.

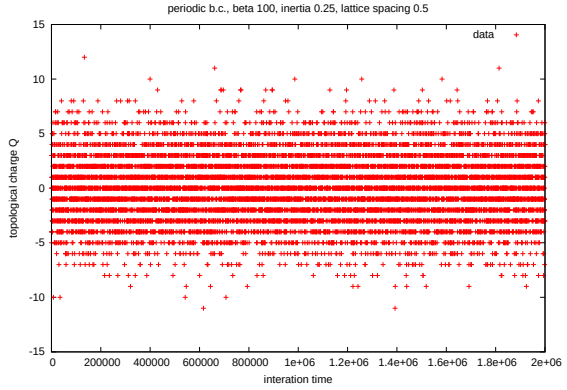


(a) $a = 0.5$, periodic

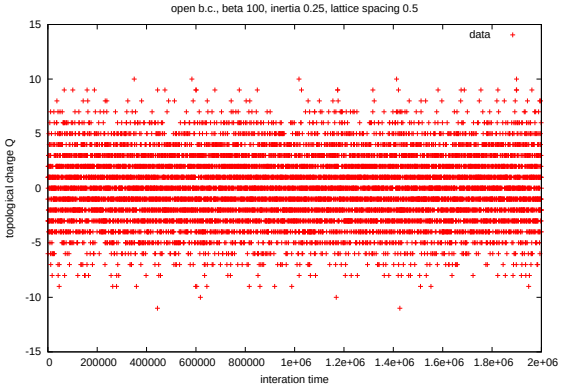


(b) $a = 0.5$, open

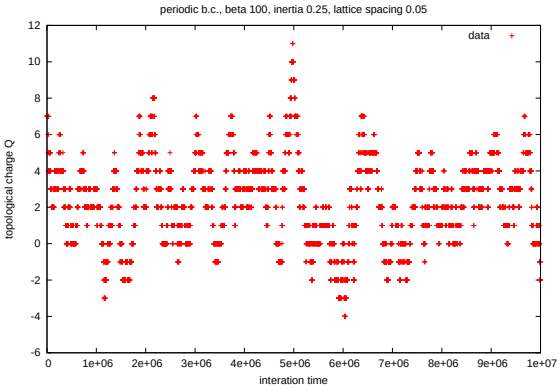


(c) $a = 0.05$, periodic

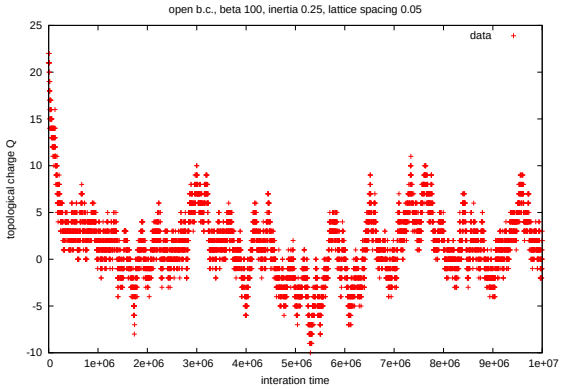


(d) $a = 0.05$, open

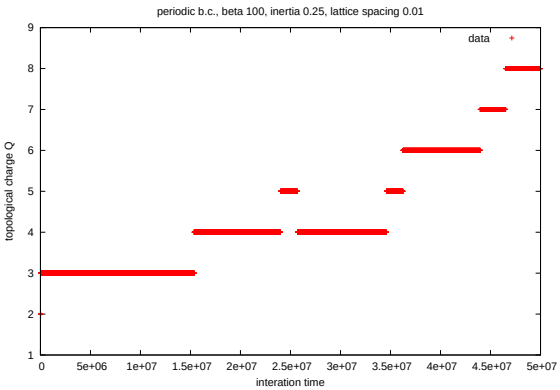


(e) $a = 0.01$, periodic

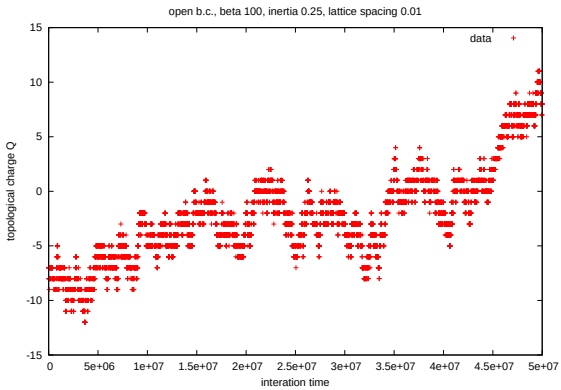


(f) $a = 0.01$, open

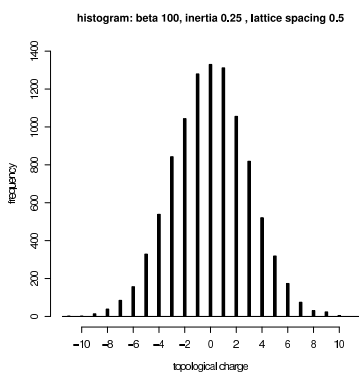


(g) $a = 0.5$

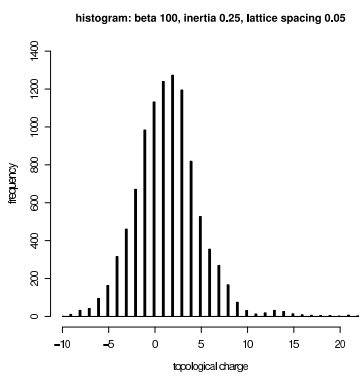


(h) $a = 0.05$

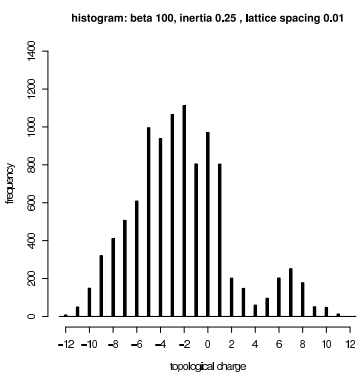


(i) $a = 0.01$

Figure 8: Topological charge as a function of iteration time for periodic b.c.'s (left) and open b.c.'s (right) for three different lattice spacings. Below: histograms showing frequency of topological charges for open boundary conditions.

This development can also be seen in the histograms in figures 8g, 8h, 8i where the frequency of the integer values of $Q$ for open b.c.'s with different lattice spacings is diplayed. On the left is the plot for the largest $a$ and it shows a Gaussian-like distribution. This is reasonable, as there is no external force acting on the system. However, going to smaller $a$'s it seems that the normal distribution is broken. This clearly indicates that for this lattice spacing there are not enough measurements to recover the underlying Gaussian distribution. This is evidently due to the extremely long auto-correlation times.

## 3.6 Energy Gap

### 3.6.1 Derivation

We are interested in the energy gap between the ground state and the first excited state, $\Delta E = E_1 - E_0$. We can relate this quantity to the moment of inertia, $I$, of the system, recalling the earlier relation

$$\xi = \frac{1}{E_1 - E_0} = 2I \tag{22}$$

First, we obtain an analytical expression for the quantity $\Delta E$.

Consider the 2-point correlation function (or propagator), $\langle q(t)q(0)\rangle = \Gamma(t)$. It is important to emphasise that this is not the same correlation function as we have previously been discussing with respect to the autocorrelation time, though they have formal similarities. This correlator is calculated over a single path in physical time, while our previous correlators are between configurations in Monte Carlo time. As we know from statistical mechanics, the expectation value in the canonical ensemble is given by

$$\langle q(t)q(0)\rangle = \mathrm{tr}\left(\frac{e^{-\beta\hat{H}}\hat{q}(t)\hat{q}(0)}{\mathrm{tr}\left(e^{-\beta\hat{H}}\right)}\right) \tag{23}$$

This is equivalent to equation 13 due to the duality we have established between the path integral and the partition function.

The operator $\hat{q}(t)$ can be written in the Schrödinger picture (recalling we are using Euclidean space, so $t \to i\tau$) using the time evolution operator, as

$$\hat{q}(t) = e^{t\hat{H}}\hat{q}e^{-t\hat{H}} \tag{24}$$

And so, taking the trace over energy eigenstates, our expectation value can be written as

$$\langle q(t)q(0)\rangle = \frac{\sum_{n=0}^{\infty}\langle n|e^{-\hat{H}\beta}e^{t\hat{H}}\hat{q}e^{-t\hat{H}}\hat{q}|n\rangle}{\sum_{n=0}^{\infty}e^{-E_n\beta}} \tag{25}$$

Where we have used the fact that

$$\mathrm{tr}\left(e^{-\beta\hat{H}}\right) = \sum_{n=0}^{\infty}\langle n|e^{-\beta\hat{H}}|n\rangle = \sum_{n=0}^{\infty}e^{-\beta E_n} \tag{26}$$

We insert another complete set of eigenstates between $\hat{q}$ and $e^{-t\hat{H}}$ to get

$$\langle q(t)q(0)\rangle = \frac{\sum_{n,m}\langle n|e^{-(\beta-t)\hat{H}}\hat{q}|m\rangle\langle m|e^{-t\hat{H}}\hat{q}|n\rangle}{\sum_n e^{-E_n\beta}} = \frac{\sum_{n,m} e^{-(\beta-t)E_m}e^{-tE_n}\langle n|\hat{q}|m\rangle\langle m|\hat{q}|n\rangle}{\sum_n e^{-E_n\beta}} \tag{27}$$

Extracting a factor of $e^{-\beta E_0}$ from top and bottom lines, then rearranging the exponents on the top yields

$$\langle q(t)q(0)\rangle = \frac{\sum_{n,m} e^{-(\beta-t)(E_m-E_0)}e^{-t(E_n-E_0)}|\langle n|\hat{q}|m\rangle|^2}{1+e^{-\beta E_1}+e^{-\beta E_2}+\dots} \tag{28}$$

$\beta$ is the formal parameter giving the volume of our time crystal (recall $\beta = N_{\text{path}}a$), and in taking the limit $\beta \to \infty$ we extract the vacuum states. Only states for which $E_m = 0$ remain, these being $|m\rangle = |0\rangle$. We then get

$$\langle q(t)q(0)\rangle = \sum_n e^{-t(E_n-E_0)}|\langle n|\hat{q}|0\rangle|^2 \tag{29}$$

For $t$ sufficiently large, the higher energy states decay away, and this simply becomes

$$\langle q(t)q(0)\rangle = \Gamma(t) = e^{-t(E_1-E_0)}|\langle 1|\hat{q}|0\rangle|^2 \propto e^{-t\Delta E} \tag{30}$$

Thus we can compute $\Gamma(t)$ over a configuration path and calculate the energy gap through

$$\Delta E = \lim_{\beta\to\infty} -\frac{1}{a}\log\left(\frac{\Gamma(t+a)}{\Gamma(t)}\right) \tag{31}$$

where $a$ is of course our lattice spacing (the smallest time increment we can take).

### 3.6.2 Results

Figure 9 shows the results for the functions $\Gamma(t) = \langle q(t)q(0)\rangle$ (where $q(t)$ is $\varphi(t)$), for different values of the lattice spacing. The x axis is scaled by the lattice spacings such that each 'length' $t$ (number of lattice points) corresponds to the same physical length. Beyond systematic or statistical deviations, the function is found as we expect not to depend on the lattice spacing. Figure 9a best demonstrates this.

However, we must still consider the lattice spacing while seeking the energy gap.

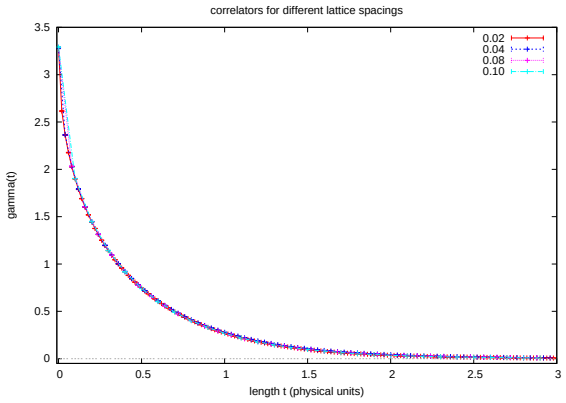


(a) At small lattice spacings we have enough points in the region of the decay to extract its properties.

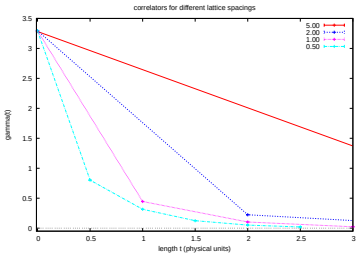


(b) Large lattice spacings do not capture the shape of the decay with sufficient accuracy.

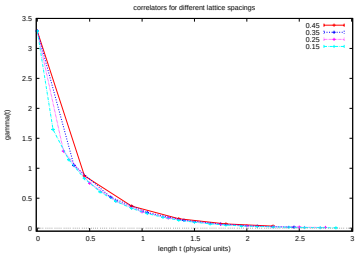


(c) Decreasing the lattice spacing shows a closer resemblance to the exponential-like decay.

Figure 9: Correlation functions $\Gamma(t) = \langle q(t)q(0)\rangle$ for different values of the lattice spacing.

Figures 9b and 9c demonstrate the issue. For an overly large lattice spacing, not even considering discretisation effects, we lack the precision required to properly observe the exponential decay of the correlation function. For a lattice spacing of 5.00 for example, we entirely miss it. We see in figure 9a how reducing the lattice spacing 'fills in' the gaps, giving a better fit for the exponential. Thus, we cannot get reliable data for the energy gap from overly large lattice spacings. We do not include the data for $a > 0.5$ when calculating the energy gap.

We now use equation 31 on our data to obtain the energy gap as a function of the length, $t$. We notice several features in figure 10.

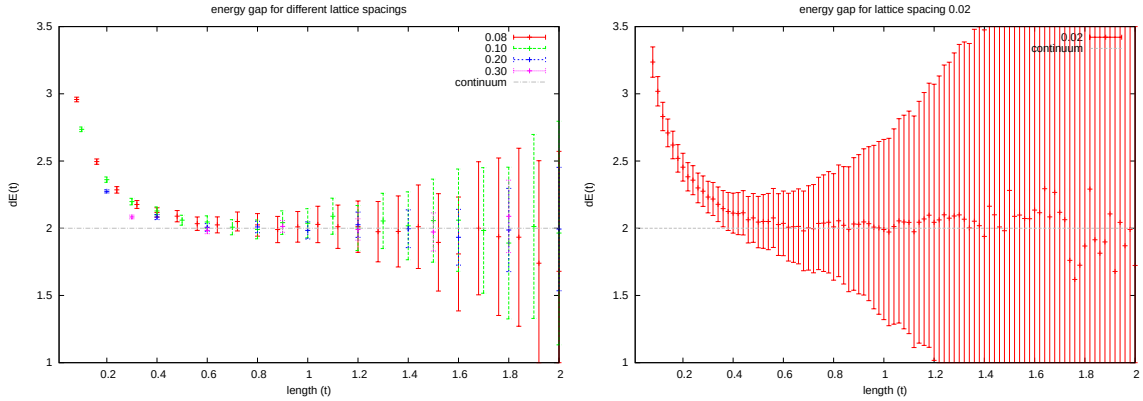


(a) Lattice spacings of 0.08, 0.10, 0.20, and 0.30.

(b) For $a = 0.02$, errors are significant.

Figure 10: The energy gap as a function of the length $t$, demonstrating plateau behaviour and errors growing with $t$. Different lattice spacings are used, with open boundary conditions, and $I$ fixed at 0.25.

- In the region $t \in (0, 0.4)$, the energy gap decays. This is due to the presence of higher energy levels as predicted by equation 29 which have not yet been suppressed. We cannot use these data points to calculate $\Delta E$.
- The energy gap then reaches a plateau. The value of this plateau is our desired value for $\Delta E$. By equation 22, since we use $I = 0.25$ here, the continuum limit value of this plateau is 2.
- Statistical fluctuations become increasingly dominant as $t$ increases, due to our correlation functions approaching 0. This is reflected in the increasing errors for larger $t$. While large lattice spacings are unsuitable for obtaining the energy gap, these statistical limitations also prevent us from gaining useful information from overly small spacings. The errors here for $a = 0.2$ are too large to determine the energy gap reliably.

Least squares fitting[9] is used on the plateau region to obtain the value of the energy gap. The results for periodic and open boundary conditions are shown in figure 11. The systematic error from the determination of the beginning and end of the plateau, which is highly subjective, is not taken into account. We see no significant difference between open and periodic boundary conditions. Once again, large lattice spacings give deviations from the continuum limit, and small spacings require better statistics to reduce errors.

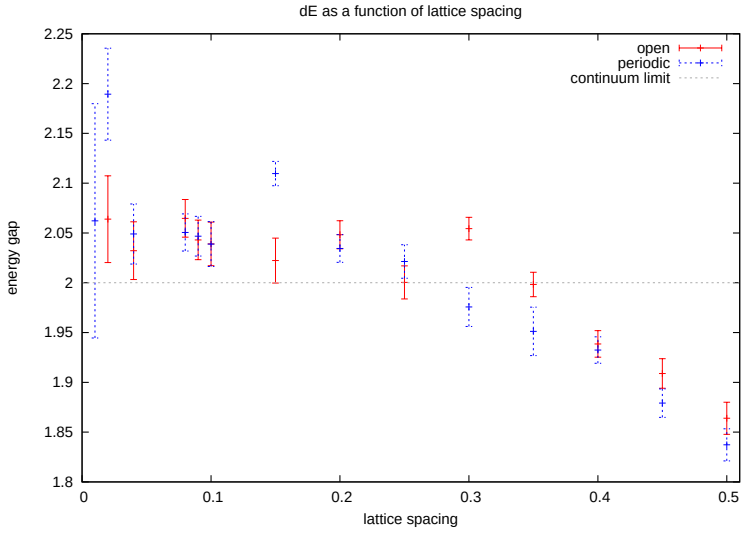


Figure 11: Results from fitting the energy gap plateau to a straight line, for various lattice spacings. $I$ is fixed at 0.25. Systematic errors from plateau determinination are neglected.

# 4 Improvements

## 4.1 Reducing the autocorrelation time - the cluster algorithm

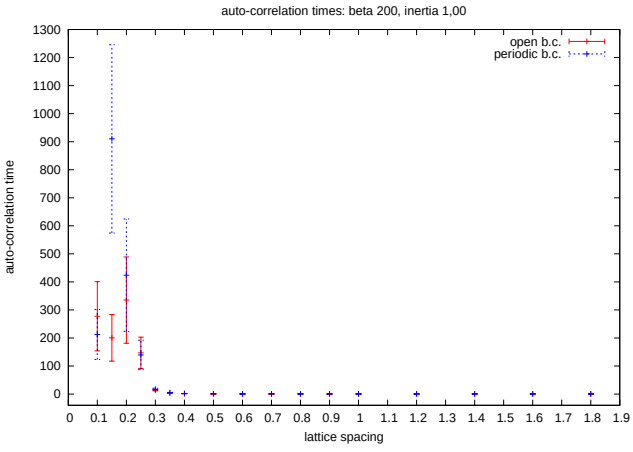


(a) The effective autocorrelation as a function of lattice spacing. Increased skipping is used at lower lattice spacings, so the true autocorrelation times are orders of magnitude higher. We see divergence of $\tau_{ac}$ for $a \to 0$. At small spacings, open boundary conditions show slightly reduced $\tau_{ac}$.

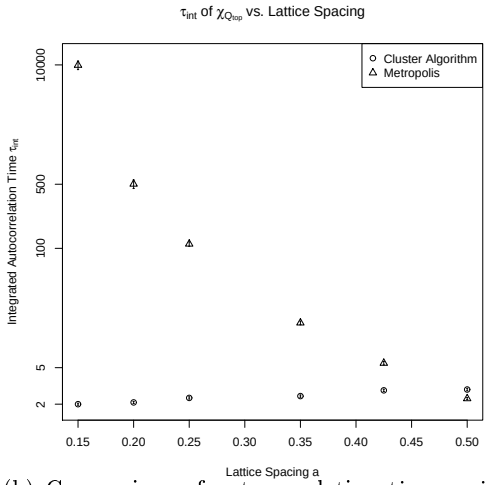


(b) Comparison of autocorrelation times using the Metropolis algorithm and the cluster algorithm. While $\tau_{ac}$ diverges for Metropolis at small lattice spacings, it *decreases* in the cluster algorithm. Figure from [10].

Figure 12: Comparing the effective autocorrelation time $\tau_{ac}$ between boundary conditions (open, periodic) and algorithms (Metropolis, cluster).

As mentioned in an earlier section, each path generated by our simulation is not entirely independent of the previous steps. In a perfect Markov process, each point of the simulation depends only on the previous point and is entirely independent of all others. That is, the effective autocorrelation length $\tau_{int} \simeq 1$. Sadly this is not true in our case. We find a growth in the effective autocorrelation length with smaller lattice spacings consistent with an exponential behaviour (figure 12a). To maintain effective statistics of 10,000

independent measurements with a lattice spacing of 0.04, we would require over $6 \times 10^9$ iterations! This is too computationally expensive. The implementation of open boundary conditions only marginally lifts the weight of this massive autocorrelation time.

We may use the *Cluster Algorithm*[11] to attempt to deal with this problem. This algorithm replaces the Metropolis algorithm in our Monte Carlo process as a method of updating our path configurations. It is of particular use in spin systems such as ours, but so far cannot be used in gauge theories.

The basic idea is to form a 'cluster' within the configuration of similar spins, and to update each spin in the cluster simultaneously. For our case, the algorithm may proceed approximately as follows

1. A random complex number is chosen, $r \in \mathbb{C}$, and a random starting point in the lattice, $i$.

2. The link probability $p_l$ between point $i$ and point $i+1$ is then calculated. This is formed by looking at the projections of $\varphi_i$ and $\varphi_{i+1}$ on $r$. A random number between 0 and 1 is generated, and the point is added to the cluster if this number is lower than $p_l$.

3. The cluster expands until a point is rejected, and then the linking stops. One can then go back to the starting point and proceed in an identical fashion, but instead looking at $\varphi_{i-1}$, that is extending the cluster in the opposite direction.

4. Once the cluster is complete, a reflection algorithm is used on all points in the cluster. This reflects each spin in $r$ (one may imagine $r$ as a vector in $\mathbb{R}^2$).

5. A new $r$ is then chosen and the algorithm begins again.

It is important to include the random number in step 2, to enable the possibility of clusters breaking up. For example, in the case of an Ising model where the spins can only take on two values, without this random step the algorithm would simply serve to eventually produce the trivial case of all spins aligned. Since we are interested in topological features, this is less than ideal!

The advantage of the cluster algorithm is that it has greatly reduced effective autocorrelation time. Figure 12b demonstrates this remarkable property. We find that for small lattice spacings, the autocorrelation time actually decreases.

## 4.2 Reducing lattice artifacts - different discretisation

From section 3.2 we see that the discretisation we use for the derivative $\dot{\varphi}$ is of order $a$. A better approximation to the continuum limit can be obtained by using a higher order approximation to the derivative (See DeGrand[6], chapter 10). For example, we can use the central difference approximation for the derivative of an arbitrary smooth function $f(x)$,

$$f_1'(x) = \frac{f(x+a) - f(x-a)}{2a} = f'(x) + \frac{a^2}{6} f'''(x) + \dots$$

This is of order $a^2$ now. However, we can do better, if we take another discretisation

$$f_2'(x) = \frac{f(x+2a) - f(x-2a)}{4a} = f'(x) + \frac{2a^2}{3} f'''(x) + \dots$$

We can then cancel the terms of order $a^2$ by forming $f_3'(x) = (1/3)(4f_1'(x) - f_2'(x))$, which is now of order $a^4$. Repeated application of this can further reduce finite lattice spacing effects, at the cost of requiring additional points to calculate the derivative.

# 5 Conclusions

During the summer student project at DESY Zeuthen, we used lattice field theoretical methods to investigate the behaviour of simple systems as well as the properties of the Metropolis Algorithm. Therefore, a significant part of the time was spent with coding simulations and data analysis aspects.

At first, we spent time on the theoretical foundations of the path integral and the connection to statistical physics, introduced by the imaginary time formalism. Furthermore, an introduction into Monte-Carlo integration was provided as well as the explanation of the Metropolis Algorithm.

The first numerical experience was gained through the example of $\langle x^2 \rangle$ in the Gaussian-like probability distribution. This gave insights into topics like thermalisation, choosing appropriate parameters and autocorrelation effects. The advantage of the system lies in the analytical solvability, which makes it easier to study effects of different parameter values. On the other hand, it was clearly demonstrated that even for this system autocorrelation is a serious issue, which needs to be taken into account if one wants to analyse more advanced systems.

A less trivial system was introduced by the 1-d $O(2)$ model which shows topological effects and required the extension of the previously developed programs. Two interesting quantities, the topological susceptibility $\chi_t$ and the energy gap $\Delta E$, were introduced and computed. The continuum limit of $\chi_t$ displays the freezing of the topological charge and the breakdown of the simulation for too small a lattice spacing. This freezing presents a real issue in lattice QCD calculations of topological systems, so observing it in this simple model is quite remarkable. Nevertheless, the simulation results agreed with the theoretical predictions in the range of lattice spacings small enough to approximate the continuum limit and large enough to avoid freezing of the topological charge.

The investigation of $\Delta E$ illustrates the theoretically predicted exponential decay of the physical correlator for the effective energy gap. Consequently, the determination of the energy gap was possible by fitting the plateau with an appropriate algorithm where, however, the systematic effect of identification of plateaus was neglected. Noting this, we find the results to be reasonable, in the sense that one sees the plateau at the appropriate level but the final values of $\Delta E$ and their errors encourage further investigation.

A last comment should be made about boundary conditions. It was suggested to use open b.c.'s to overcome the problem of frozen topological charges observed in periodic b.c.'s. It was possible to verify, to some extent, that this is indeed the case and one is able to obtain reliable data for smaller lattice spacings. However, even this new approach is ultimately limited by the same problems as the periodic b.c.'s.

In summary, we have investigated some of the methods of lattice QCD by simulating relatively simple systems. These concepts are extended to real physical systems (as seen

in the Witten-Veneziano formula) in real lattice QCD work. We hope that the findings presented here, in particular the freezing of the topological charge and overcoming this and massive autocorrelation times by the cluster algorithm, can help to alleviate the topological charge freezing also observed within QCD. One interesting aspect of our work would be to study the correlation between the freezing of the topological charge and the physical observables, such as the energy gap. Such a study goes beyond the scope of this summer student work however, but could be addressed in the future.

## Acknowledgements

Finally, we would like to thank our supervisor Karl Jansen for his patience, guidance and devoting so much time to us and to the rest of the summer students. In addition, we are very grateful for the support and kindness we experienced from the PhD students Elena Garcia Ramos and Andreas Nube.

## References

[1] M. Creutz and B. Freedman, *A Statistical Approach to Quantum Mechanics*, Annals of Physics, **132**, 427-462 (1981).

[2] Yorikiyo Nagashima, Yoichiro Nambu, *Elementary Particle Physics Volume 1: Quantum Field Theory and Particles*, (WILEY-VCH, 2010)

[3] W. H. Press, S. A. Teukolsky, W. T. Vetterling, B. P. Flannery, *Numerical Recipes in FORTRAN - The Art of Scientific Computing, 2nd Ed.* (Cambridge University Press, 1992)

[4] G. M. Buendía, *Comparison between the Langevin and the hybrid simulation techniques for a free field theory*, J. Phys. A: Math. Gen. **22**, 5065-5072 (1989).

[5] T. Cheung and L. Li, *Gauge theory of elementary particle physics*, (Oxford University Press, 1984)

[6] T. DeGrand and C. DeTar, *Lattice Methods for Quantum Chromodynamics*, (World Scientific, 2006)

[7] W. Bietenholz, U. Gerber, M. Pepe, U.-J. Wiese, *Topological Lattice Actions*, arXiv:1009.2146v4 [hep-lat] (20 Dec 2010)

[8] M. Lüscher, S. Schaefer, *Lattice QCD without topology barriers*, CERN-PH-TH-2011-116, 26pp (May 2011)

[9] W. H. Press, S. A. Teukolsky, W. T. Vetterling, B. P. Flannery, *Numerical Recipes in C - The Art of Scientific Computing, 2nd Ed.* (Cambridge University Press, 1992)

[10] A. Nube, private communication.

[11] U. Wolff, *Critical Slowing Down*, Nuclear Physics B (Proc. Suppl.) **17**, 93-102 (1990).